Conf-830439--5

HYDRODYNAMICS OF ADIABATIC INVERTED ANNULAR FLOW - AN EXPERIMENTAL STUDY

CONF-830439--5

DE83 011748

George De Jarlais and Mamoru Ishii
Reactor Analysis and Safety Division
Argonne National Laboratory
9700 South Cass Avenue
Argonne, Illinois 60439, U.S.A.

ABSTRACT

For low-quality film boiling in tubes or rod bundles, the flow pattern may consist of a liquid jet-like core surrounded by a vapor annulus, i.e., inverted annular flow. The stability, shape, and break-up mechanisms of this liquid core must be understood in order to model correctly this regime and to develop appropriate interfacial transfer correlations. This paper reports on a study in which inverted annular flow was simulated in an adiabatic system. Turbulent water jets, issuing downward from long-aspect nozzles were enclosed within cocurrent gas annuli. Jet-core diameter and velocity, and gas-annulus diameter, velocity, and species were varied, yielding liquid Reynolds numbers up to 33,000, void fractions from 0.29 to 0.95, and relative velocities from near zero to over 80 m/s. Jet-core break-up lengths and, secondarily, core break-up mechanisms, were observed visually, using strobe lighting. Still photographs using a 3-microsecond flash exposure were taken, as the primary source of break-up mechanism information, to observe core surface disturbance wavelengths and dispersed core droplet sizes, and as a secondary source of break-up length data. This experiment is unique in that extensive data for the disintegration of confined coaxial jets (liquid core and gas annulus) have been obtained.

1. INTRODUCTION

Inverted annular flow occurs in confined boiling heat transfer systems, when low quality flow is coupled with post-CHF film boiling. The resulting flow pattern is a liquid core surrounded by a blanketing annulus of vapor. Understanding the hydrodynamics of this flow regime is of practical concern, since inverted annular flow may occur in light water reactor accident situations, in which, after loss of core coolant, core reflood brings coolant into the confined regions between very hot fuel rods [1]. Inverted annular flow may also occur in the transient operation of cryogenic heat transfer or conveyance systems, such as those found in rocket propulsion applications [2].

Given the importance of inverted annular flow specifically, and post-CHF heat transfer phenomena in general, a great deal of work has been done in this area in the last 30 years [1,3]. Yet our understanding of the basic post-CHF hydrodynamics, especially those of inverted annular flow, has not progressed sufficiently, in part because, in typical film boiling experiments, control and measurement of the flow parameters necessary for such an understanding is difficult, if not impossible, to achieve. Confined geometries, and the minimum temperatures and heat transfer rates required for film boiling, often

prevent even simple flow visualization. There have been, however, a few inverted annular flow studies in which limited hydrodynamic information was obtained. Simple flow regime observations were made by Laverty and Rosenow [4] and by Kalinin et al. [5] in which the transition of inverted annular flow to inverted slug or dispersed droplet flow was noted. In the analytical study by Jensen [6], break-up lengths of the inverted annular flow liquid core were calculated, along with surface wavelengths. In the transient film boiling experiment of Kurilenko et al. [7] and the steady state film boiling experiment of Ottosen [8], flow regime observations and void fraction measurements were made. Finally, in the FLECHT SEASET series of tests, such as those reported in [9], dispersed droplet sizes and velocities were measured at distances well beyond the CHF point.

As a result of our limited understanding of post-CHF hydrodynamics, including those of inverted annular flow, many film boiling applications are amenable to only limited analysis at present. One example of this can be seen in large-scale LWR safety codes such as TRAC and RELAP, which are essentially constrained by the not-well understood two phase thermo-hydraulics under various accident conditions.

2. SIMULATED INVERTED ANNULAR FLOW EXPERIMENT

In light of the experimental difficulties associated with hydrodynamic studies of inverted annular flow film boiling, an adiabatic simulation of inverted annular flow was performed in this study. This simulation was accomplished by enclosing turbulent water jets, issuing from long aspect nozzles, within cocurrent annular gas jets flowing in transparent tubes. Such a simulation was suggested by Jensen [6], who noted the similarities between the liquid core stability of inverted annular flow and the stability of liquid jets. In this simulation, fluid properties, velocities, and initial geometries were easily controlled and measured. In addition, with no need to maintain film boiling heat transfer, ambient temperatures could be used, steady state flow was assured, and the flow pattern up to the point of core break-up was easily observed.

The experiment was performed in a set of five test series, each with fixed values for initial jet core diameter, D_J, and gas annulus outer diameter, D_O. Within each series, jet core velocity, v_J, and gas annulus velocity, v_G, were varied. In addition, for two of the test series, gas species (and therefore density, ρ_G) was also varied. The series of tests performed are summarized in Table 1.

All tests were performed near atmospheric pressure, with flow directed downward. Upward flow was attempted, but the use of low velocity liquid jets, coupled with easy wetting of the gas annulus outer wall (which would not occur

Table 1. Test Series Geometries, Gas Species

Test Series	Nozzle Diameter (cm)	Nozzle Length (cm)	Outer Diameter (cm)	Initial Void Fraction	Gas Species
A7	0.425	41.	1.66	0.934	Nitrogen
B2	0.763	46.	1.36	0.685	Nitrogen, Helium, R-12
B3	0.902	67.	1.36	0.560	Nitrogen, Helium, R-12
C1	0.604	37.	0.90	0.549	Nitrogen
C2	0.763	46.	0.90	0.281	Nitrogen

in true inverted annular flow film boiling) made this impractical. Even with downward-directed flow, wall wetting by the dispersed liquid core made data acquisition difficult at high gas flowrates.

For each trial run, jet core break-up length, L_B, was determined from strobe-aided visual observation of the flow pattern, with supplementary break-up length information supplied by still photographs. Jet core break-up mechanisms were also determined for each trial run, from still photographs supplemented by visual observations. In addition, core surface disturbance wavelength and dispersed core maximum droplet diameter data were obtained for many trial runs, where photographs provided such information.

The apparatus and procedures for the experiment are described in the following sections.

2.1. Apparatus

The experimental test system is shown schematically in Fig. 1, and a drawing of the basic test section is shown in Fig. 2.

The test section. The test section used to simulate inverted annular flow conditions consisted of three basic components: a lucite base with integral gas plenum, stainless steel tube water nozzles, and Pyrex tubing forming the outer surface of the gas annuli. The water nozzles were coaxially centered within the Pyrex tubing, and gas flow was introduced, from the gas plenum, into the annular gap between the stainless steel and Pyrex tubes. The test section was designed so that various-sized water nozzles and Pyrex tubing could be used to give a range of initial dimensions and void fractions. Test section construction was such that all water nozzles had an aspect ratio (length divided by inner diameter) of at least 50 so that entrance region effects would be minimal at the nozzle exit. Similarly, the length of unobstructed gas flow in the annulus between the stainless steel and Pyrex tubes, upstream of the water nozzle exit, was a minimum of 50 times the steel/Pyrex gap width.

Design and construction of the test section was relatively simple. The base and gas plenum were fabricated from lucite plate and tubing. The gas plenum was filled with coarse stainless steel wool to eliminate large-scale vortices in the gas flow entering the test section, thereby promoting a uniform flow pattern into the gas annulus.

The water nozzles were fabricated from thin-walled (.155 and .255 mm wall thickness) stainless steel tubing. These nozzles were hand-ground, so that tube wall thickness near the nozzle exit decreased smoothly, ending in a knife edge at the exit itself. With this form, no sudden gas flow area change occurred at the nozzle exit, minimizing entrance effects at the start of the simulated inverted annular flow region of the test section. Six spacing pins, made of 1.27 mm diameter copper wire, were soldered onto each steel tube to coaxially center each nozzle tube within an outer tube of Pyrex. To allow for slight variations in D_o along the Pyrex tube length, these pins were designed to act as cantilevered beams, flexing slightly as the steel nozzles were positioned in the Pyrex tubes. Three of these pins were placed near the nozzle exit, equally spaced about the tube circumference, at a distance from the exit at least 50 times the width of the Pyrex/stainless steel annular gap for each test series geometry. This pin/nozzle exit distance was established to allow dissipation of gas flow disturbances caused by the spacing pins, prior to the region of the test section in which the simulated inverted annular flow occurred. The second set of three spacing pins was placed 3 to 7

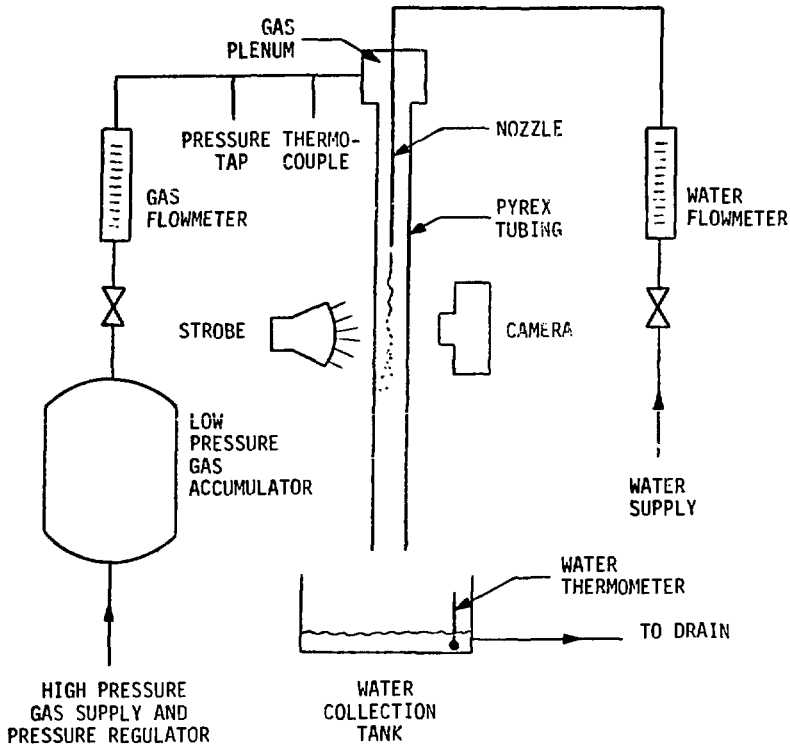

Fig. 1 Schematic Diagram of Test Apparatus

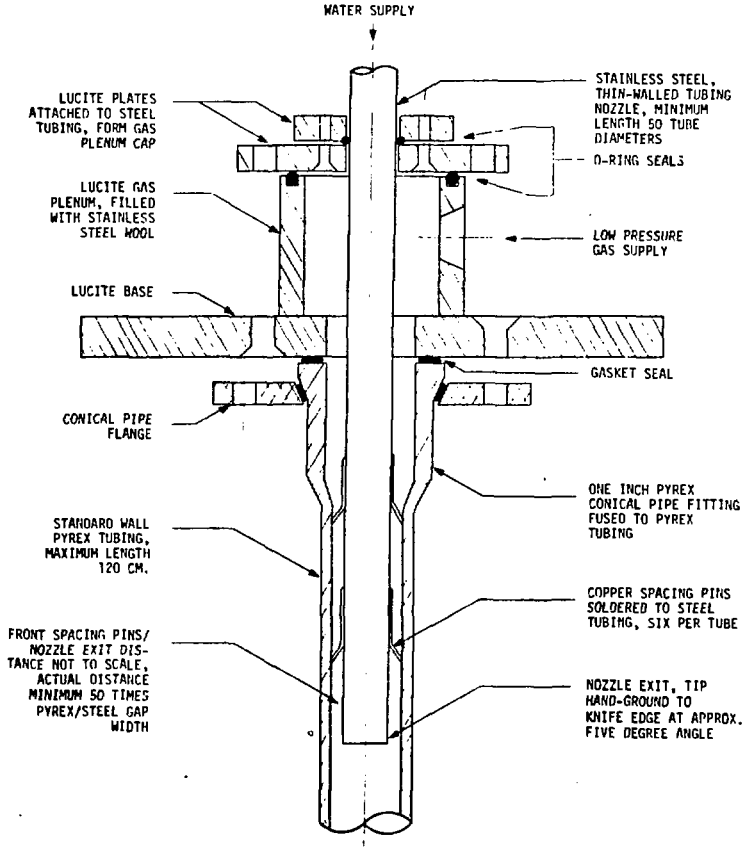

Fig. 2 Drawing of Test Section

cm behind the first set, with the pins spaced about the tube circumference in positions rotated 60° from the first set of pins. Copper spacing pins were not, however, used to align the nozzle of the C2 test series in which the annular gap width was only 0.53 mm. For this narrow gap, the spacing pins became too stiff to accommodate diameter variations (typically ±0.05 mm) in the Pyrex tube. For this test series, coaxial centering was accomplished by placing three narrow ridges, axially oriented, at 120° intervals about the nozzle tube circumference. These ridges consisted of several layers of thin plastic adhesive tape (thickness of 0.05 mm), the number of such layers varied to control alignment, placed over a strip of fabric adhesive tape, which could compress slightly in response to varying Pyrex tube diameter.

The Pyrex tubing of the test section was standard wall stock (1.0 or 1.2 mm wall thickness). At one end of each tube, a 1 inch, Pyrex conical pipe end fitting was fused in place. At the fused tube/pipe joint, a minimum ID equal to the Pyrex tube ID, D_o, was maintained, so that the stainless steel nozzle, with spacing pins (or ridges), could easily be inserted. This conical pipe end fitting was bolted onto the lucite base plate, using an aluminum conical pipe flange. To minimize vibration of the Pyrex tube, it was clamped in place at its free end (the test section exit) and at a point slightly upstream of the water nozzle exit. Standard Pyrex tubing lengths of 120 cm were used for most trial runs. For a limited number of trials in the B2 test series, however, a shortened test section, using only 32 cm of Pyrex tubing, was developed. With this shorter test section, the distance from the core jet break-up point to the test section exit could be minimized, with actual break-up/section exit distances varied by the positioning of the water nozzle within the Pyrex tube. Observations of the dispersed liquid resulting from core break-up could then be made at the test section exit. Such observations, it was found during preliminary experimental trials, could not be made along the test section proper, since liquid of the dispersed core rapidly wetted the inner wall of the Pyrex tube, forming a wavy, opaque, annular film of liquid. The exit of this shortened test section was therefore designed to divert this annular liquid film radially, and allow an unobstructed view of the dispersed slugs or droplets remaining after core jet break-up. This radial diversion of the liquid annular film was accomplished by flaring the free end of the Pyrex tubing outward, and placing a concentric lucite cone, with an aperture equal to D_o, within this Pyrex flare. Water flowing as a film down the Pyrex wall at the test section exit would then flow through the conical annulus of the Pyrex/lucite gap, and away from the test section exit.

Support Systems. Gas and water delivery systems were developed, to supply fluid flows to test section. And, to observe the hydrodynamic behavior of the simulated inverted annular flow within the test section, visual and photographic observation systems were developed as well. These systems, like the test section itself, are shown schematically in Fig. 1.

Nitrogen and helium gas were obtained from high pressure supply tanks. These tanks were connected to a high pressure manifold, from which a pressure reducing valve fed gas into a 0.3 m^3 low pressure gas accumulator maintained at approximately 0.4 MPa. For R-12 (CCl_2F_2) flows, gas was fed directly from supply tanks into the gas accumulator. From this accumulator, gas flowed through a needle valve controlling the flowrate, and then through one of three variable area flowmeters. Use of three flowmeters (cumulative range 0.02-6.3 ℓ/s nitrogen at STP) was necessary to allow for large variations in initial gas flow areas and gas velocities. Gas pressure and temperature were measured at the flowmeter exit. From the flowmeter, gas then flowed into the test section gas plenum, through the annular gap between the water nozzle and the Pyrex tubing, and into the similar annular gap between the Pyrex tubing and

turbulent water jet issuing from the water nozzle. Gas was vented directly from the test section exit.

Water, supplied from a potable water system, flowed through a needle valve controlling the flowrate, and then through a variable area flowmeter (range approximately .02-.3 ℓ/s water at 25°C). The water then flowed into the stainless steel long aspect nozzle of the test section. At the test section exit, the water flow was collected in a small plastic tank fitted with a drain line and a fully-submersed thermometer used to measure water temperature.

To serve as a reference length scale for all observations, a transparent ruler marked with 1 mm divisions was clamped along the entire Pyrex tubing length. The Pyrex tubing was then centered in a square tube of lucite, 10 cm wide and 120 cm long. The sides and portions of the back of this square tubing were made opaque, to minimize all lighting of the test section except from directly behind. An externally triggered strobe light was placed behind the test section, on an adjustable mounting bracket which allowed the strobe to traverse the entire Pyrex tubing length. This strobe generated a 3 μs, 0.5 w-s pulse of light, at a maximum rate of 700 pulses/minute. The test section was illuminated by light from this strobe directed onto a white background, mounted on the same bracket as the strobe light and placed approximately 15 cm behind the test section centerline. For visual observations, the strobe was triggered by a manually operated, hand-held switch. Photographic observations of jet core break-up characteristics were made with a Graphlex 4 x 5 camera, using ASA 3000 black and white Land film. The camera was mounted in front of the test section, on an adjustable-height tripod which allowed the camera, like the strobe, to traverse the entire Pyrex tubing length. Lighting for the photographs was provided by the white background illuminated by the strobe light. For the 3 μs exposure times, made possible by the strobe lighting and ASA 3000 film, resolution of small diameter, high velocity droplets was possible (a 0.1 mm drop traveling at 30 m/s will only travel 0.09 mm over a 3 μs time interval). The camera was positioned so that approximately 10 cm of test section could be seen in each photograph.

2.2. Test Procedures

Through the five test series, 741 trial runs were performed using the standard length test section and 17 trial runs were performed using the shortened B2 test section with the 32 cm long, flared Pyrex tubing. Table 2 summarizes the range of gas and liquid velocities, and resultant core break-up lengths, for the various test series. Velocities given are those calculated at the water nozzle exit.

Table 2. Test Series Summary

Test Series	Number of Runs	Gas Species	v_J (m/s)	v_G (m/s)	L_B (cm)
A7	137	Nitrogen	1.4-8.6	0-41	1.7-49
B2	111	Nitrogen	0.7-3.4	1-30	2.2-73
B2	49	R-12	0.7-2.7	4-18	1.6-26
B2	56	Helium	0.7-2.7	24-91	1.6-23
B3	134	Nitrogen	0.9-2.9	1-36	1.8-85
B3	22	R-12	1.4-2.4	5-18	1.2-21
B3	27	Helium	1.4-2.4	25-88	1.4-17
C1	153	Nitrogen	1.1-4.3	2-30	1.0-53
C2	69	Nitrogen	0.7-3.4	2-20	1.2-51

For each test series, vertical alignment of the test section and coaxial alignment of the stainless steel and Pyrex tubing were first established by adjusting the mounting of the Pyrex tubing and the heights of the spacing pins (or ridges) attached to the stainless steel tubing. Such alignment was verified visually and photographically, by observing symmetry within the test section during: 1) the rotation of the water nozzles within the Pyrex, 2) the flight of droplets formed by dripping flow at the nozzle exit, 3) the flight of high velocity liquid jets with minimal gas flow, and 4) the break-up moderate velocity liquid jets with high gas flow.

Once alignment was accomplished, data acquisition could commence. Typically, a series of trial runs were performed at a fixed liquid flow rate and fixed gas species, with monotonically increasing or decreasing gas flow rates. For each trial run, gas temperature, pressure and flowmeter reading, liquid temperature and flowmeter reading, and atmospheric pressure were recorded.

Visual observation of jet core break-up length was then made. The strobe light mounting bracket was gradually moved along the test section length, and the strobe triggered periodically until the region of the test section containing the break-up point was located. The strobe was then triggered in short bursts of 10-20 individual flashes at rates of approximately 150 flashes/minute. At each flash, the point of jet core break-up was noted, using the transparent ruler clamped to the test section as a reference. After 100-200 individual strobe flashes, an average jet core break-up length could normally be ascertained. The difficulties encountered in establishing this break-up length were two-fold. First, break-up length was not limited to a single, unique value for a given set of flow conditions. Rather, break-up occurred within a range of distances downstream of the nozzle exit. This variability in break-up length was similar to that observed by investigators of free-jet break-up. For example, Iciek [10] observed variations in free jet break-up length of up to ±25%, while Chen and Davis [11] found that 150 separate jet length observations had to be made in order to establish an average break-up length, with a 5% probability level and a tolerance of three jet diameters. Secondly, at high gas flowrates, the point of jet break-up became less well defined, as the growth of small volume roll waves on the jet surface, with subsequent droplet entrainment and core surface distortion, created a very complicated flow field. The actual point of jet core break-up became a matter of definition. For low void fractions, the break-up point was defined as the point at which the disintegrating jet continuously wetted the Pyrex, while for high void fractions, the break-up point was defined as the point at which core surface area increased rapidly, due to the growth of large amplitude roll waves, resulting in deformation of the jet core into sheet-like segments. For these flow conditions, flow field visibility was limited by the wetting of the Pyrex wall by roll wave crests and entrained droplets.

When possible, visual observation of jet core break-up mode, or mechanism was also made, using the strobe light. For flow conditions in the transitional regions, where two competing break-up modes were present, such visual break-up mode determinations were difficult to make. When a single mechanism of jet break-up was dominant, however, visual determination of this mechanism could normally be made. When such a visual determination could not be made, one or more photographs were taken of the flow field, near the break-up point. Photographs were also taken at selected high gas velocities, to clarify the definition of the core break-up point. And, finally, one or more photographs were normally taken at every second or third gas velocity value, as gas velocity was monotonically increased or decreased for a given liquid jet velocity. The number of photographs taken at each selected set of flow

conditions varied from one up to four or five, depending upon the complexity of the flow field and the usefulness of the information obtained from the photographs.

When photographs taken at the selected flow conditions displayed a relatively representative, uniform surface disturbance wavelength, this wavelength was measured, using as a reference the transparent ruler visible in each photograph, and recorded. In addition, the distance from the liquid nozzle exit to the point of photographic observation was recorded, again using the transparent ruler as a reference.

When photographs taken at the selected flow conditions depicted small droplets being sheared from the jet core surface, the maximum droplet size observed was measured, using the transparent ruler as reference, and recorded, along with the nozzle exit/observation point distance. Typical photographs contained only three to six visible droplets. Size measurements were made by comparing the droplets, under slight magnification (~3X), to a series of templates with widths starting at 0.1 mm and increasing in 0.1 mm increments. For spherical droplets, it was possible to measure droplet diameters within an accuracy of roughly 0.05 mm.

For the 17 trial runs using the B2 test series shortened test section, an additional parameter to be varied was the distance from water nozzle exit to the test section exit. Photographs for these trial runs were normally taken at the test section exit. These photographs usually depicted large sheets and ligaments of liquid resulting from core break-up, and maximum droplet diameters were not recorded. However, at the largest nozzle exit/section exit distances, only dispersed droplets were observed. For one such trial, trial B2-905, all dispersed droplet diameters were measured and recorded. Flowrates of water flowing as dispersed phase in the gas, and flowing as a liquid film on the inside wall of the Pyrex tubing, were measured and recorded for these 17 trial runs.

3. EXPERIMENTAL RESULTS

This adiabatic simulation of inverted annular flow produced a great deal of data on core jet break-up length, break-up mechanisms, interfacial surface characteristics, and dispersed core droplet sizes. Initial results are summarized in the following paragraphs, while a complete tabulation of the experimental results may be found in [12].

3.1. Break-up Length

Typical break-up length data are plotted in Figs. 3 and 4. The data may be divided into two regions, one in which gas flow conditions (v_G, ρ_G, α) had no influence, and a second in which gas flow did influence break-up length. In this first region,

$$L_B \sim v_J^{0.5} \tag{1}$$

This dependence is similar to that observed by Miesse [13] and by Grant and Middleman [14], who found L_B to be proportional to $v_J^{0.4}$ and $v_J^{0.6}$, respectively, for turbulent liquid jets not subjected to significant interfacial drag.

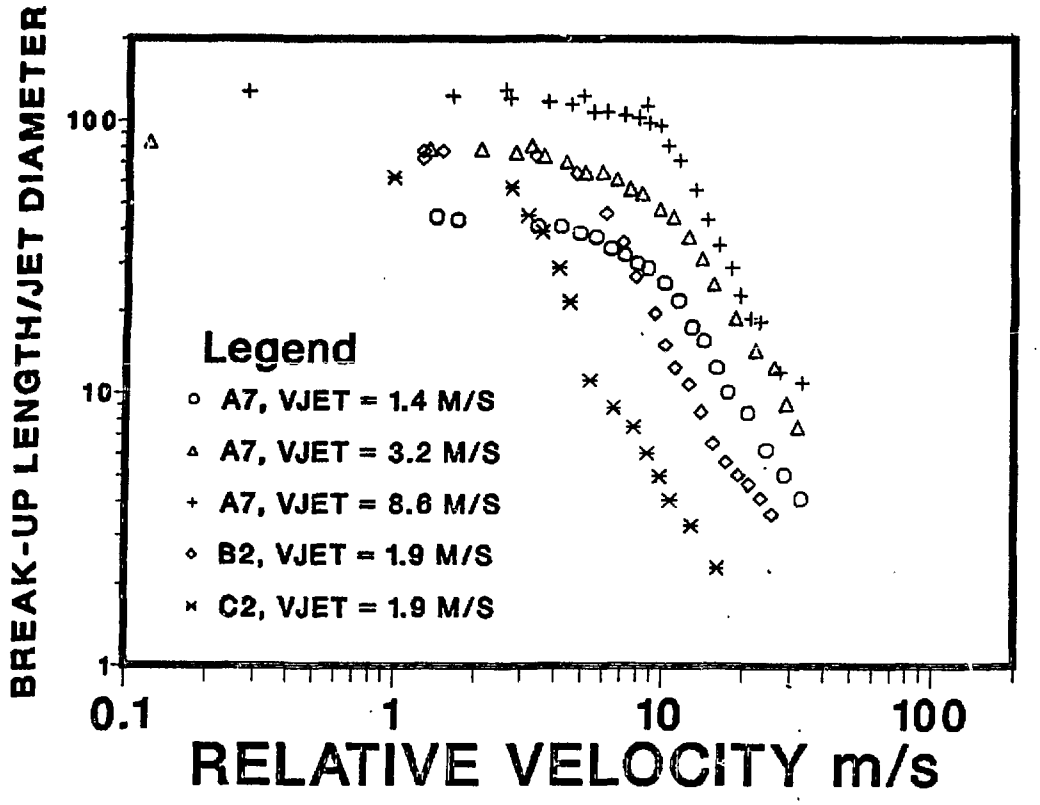

Fig. 3 Break-up Length, Nitrogen Gas, See Table 1 for α, D_0, D_J Values

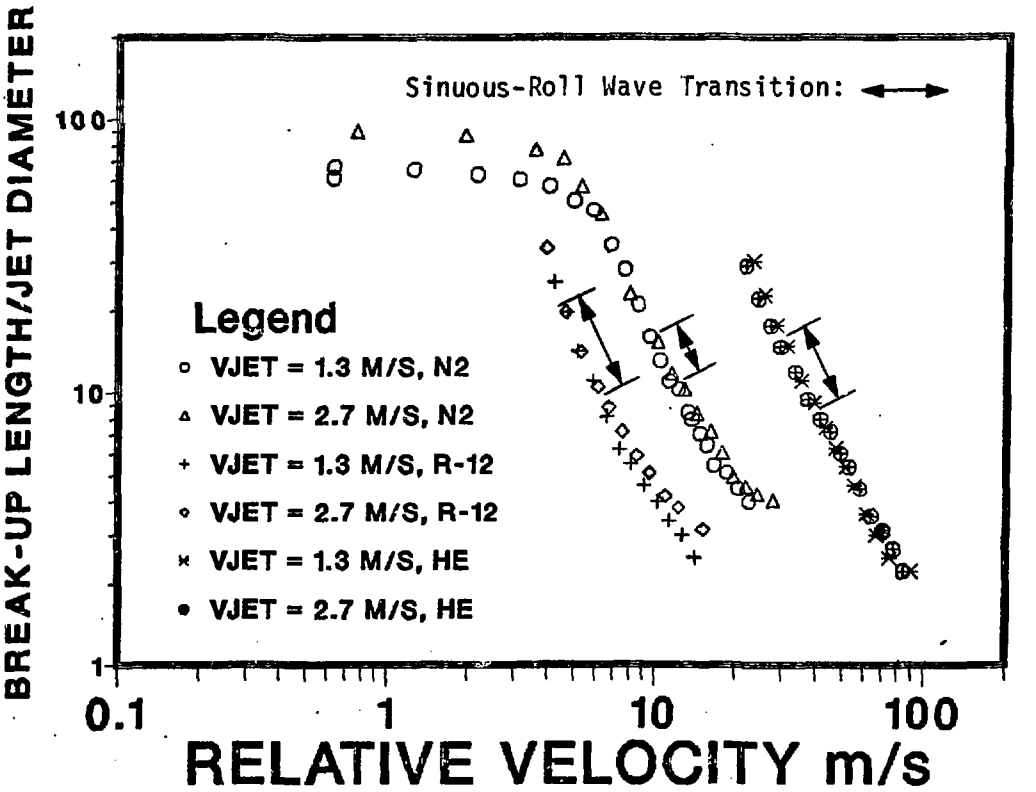

Fig. 4 Break-up Length, Break-up Mechanism, B2 Data, See Table 1

For the region in which gas flow conditions affected break-up length, it appears that

$$L_B \sim v_J^{0.5} \, v_{rel}^{-1.3} \tag{2}$$

where v_{rel} is the absolute value of $(v_G - v_J)$. This is similar to the results of Jensen's [6] calculations, which, in rough approximation, show that

$$L_B \sim v_J^{1.0} \, v_{rel}^{-2.8} \tag{3}$$

for laminar, planer jets, and is in close agreement with the results of Lienhard and Day [15], who found L_B to be proportional to v_J^{-1} in the drag-induced break-up region of free jets (where $v_{rel} = v_J$). The experimental data, like the calculations of Jensen, show that L_B decreases with decreasing void fraction, or with increasing gas density.

3.2. Break-up Mechanisms

Three different break-up mechanisms, varicose deformation of the liquid core, sinuous deformation of the liquid core, and roll wave entrainment dispersion of the liquid core, were observed in this experiment, just as three different free jet break-up mechanisms (varicose deformation, sinuous deformation, and atomization) have been observed [16]. See Fig. 5 for a drawing of these mechanisms. The first mechanism, varicose deformation, was characterized by the growth of axisymmetric waves on the jet core, resulting in alternating points of core expansion and contraction. This break-up mode resulted in transition from inverted annular flow to inverted slug flow, with the liquid slugs having a volume equal to that of a cylinder with diameter equal to initial jet diameter, and length equal to the varicose wavelength with the largest rate of growth. Varicose break-up occurred in the region where gas flow conditions had no effect upon jet core break-up length. See Figs. 3 and 4.

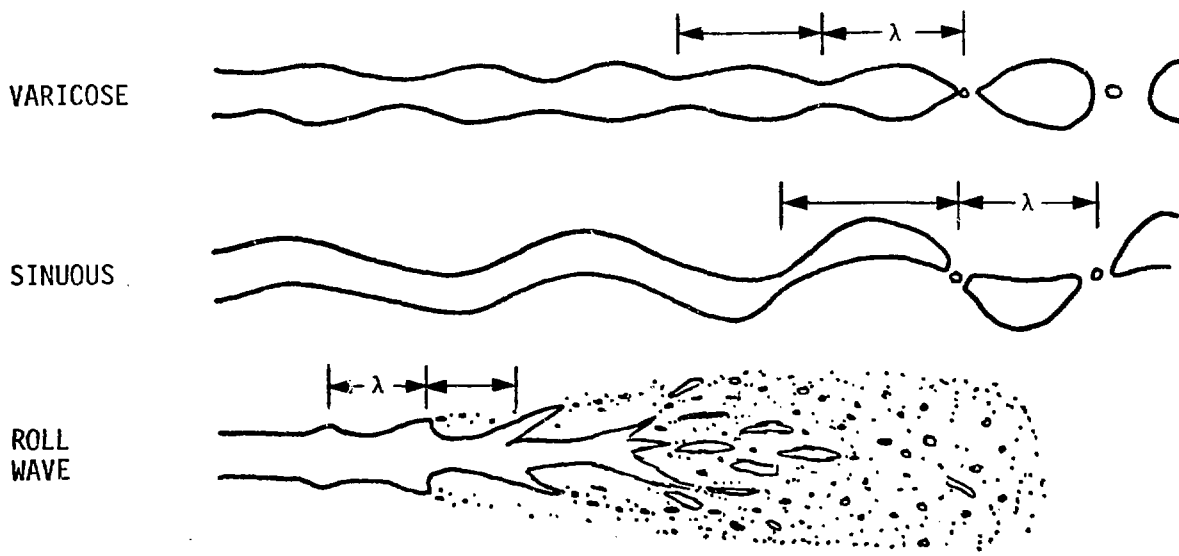

Fig. 5 Jet Core Break-up Mechanisms

The second mechanism of core break-up, sinuous deformation, is characterized by the growth of asymmetric waves which deform the jet core into a snake-like shape. The break-up mode again results in a transition from inverted annular to inverted slug flow. Sinuous break-up first occurs when gas flow conditions began to reduce core break-up lengths.

The third mechanism of jet break-up observed in these experiments is that of roll wave entrainment resulting in a transition from inverted annular flow to dispersed droplet flow. Roll waves first appeared on the crests of sinuous waves, while at higher relative velocities roll waves caused break-up before the core exhibited any sinuous behavior. A single roll wave often developed over a substantial portion of the jet circumference, deforming into a thin, skirt-like sheet. Ligaments or individual droplets could be seen being sheared from the roll wave crests. Except at the highest void fractions, it was not possible to view the entire dispersal of the liquid jet core, due to wall wetting. Because of this, it is possible that after initial core disruption due to large amplitude roll waves, other unobserved mechanisms might also have contributed to droplet formation. The transition from sinuous deformation to roll wave entrainment break-up is indicated in Fig. 4. From Fig. 4 it is apparent that this transition region is roughly determined by the value of $(\rho_G v_{rel}^2)$. This result is similar to that found by Ishii and Grolmes [17] for inception of roll wave entrainment in annular flow, and that found by Mishima and Ishii [18] for inception of slug formation in horizontal stratified flow. The value of $(\rho_G v_{rel}^2)$ at the transition from sinuous to roll wave break-up depends upon void fraction, with increasing void fraction requiring larger values of $(\rho_G v_{rel}^2)$. This result is also similar to that found by Mishima and Ishii [18].

3.3. Jet Core Surface Characteristics

Surface conditions were observed for varicose, sinuous, and roll wave break-up of the jet core. Representative wavelength are plotted versus relative velocity in Fig. 6. For varicose break-up, an average wavelength of

$$\lambda = 5.8\ D_J \tag{4}$$

was observed. This is similar to the value of $4.51\ D_J$ predicted by Rayleigh [19] for varicose break-up of laminar free jets. In the drag-induced break-up regions (sinuous and roll wave break-up), wavelengths steadily decreased with increasing values of $(\rho_G v_{rel}^2)$.

Regarding the shapes of the surface waves observed, the following generalizations can be made. For low void fractions, roll waves were limited in amplitude by the proximity of the Pyrex wall. At higher void fractions, however, roll waves were able to grow to large dimensions, sometimes deforming the jet into sheets and ligaments with no discernible cylindrical core. This large deformation normally occurred within the last few jet diameters of intact jet core length. Near the inception of roll waves, jets under sinuous break-up no longer had a smooth sinusoidal shape. Wave crests became pointed, and downstream surfaces of each wave were at much steeper slopes than upstream surfaces.

3.4. Dispersed Core Droplet Size

As previously discussed, varicose and sinuous core jet break-up resulted in the formation of large liquid slugs. Subsequent disintegration of these

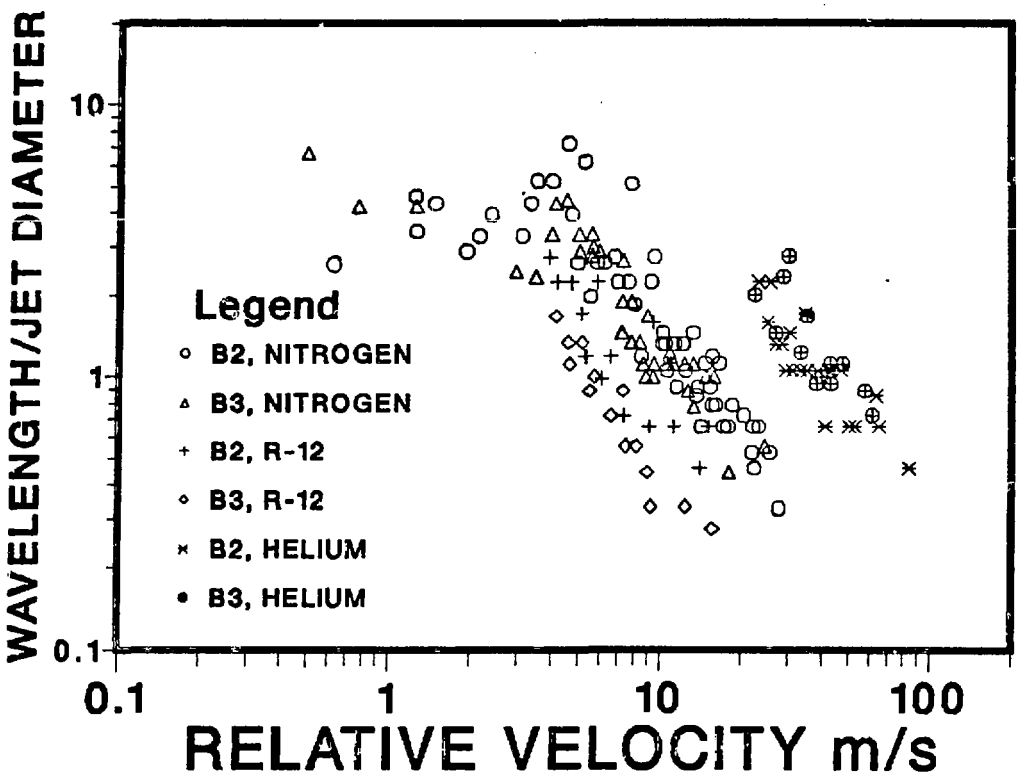

Fig. 6 Jet Core Surface Wavelength, Various v_J Values, See Table 1

slugs was not observed in this experiment, due to wall wetting and limited observation length beyond the point of core break-up.

For roll wave entrainment jet break-up, little droplet size data could be obtained, since roll waves and their entrained droplets wetted the wall after the point of jet break-up, creating an annulus of rough wavy liquid which obscured the dispersed droplet core. However, a limited number of photographs were obtained in which droplets were observed immediately after being sheared from roll wave crests. From these photographs, maximum droplet diameters were measured, within an accuracy of ~0.05 mm. Most droplet diameters were within the range of 0.25-0.55 mm for flows ranging from early roll-wave inception to well established roll wave entrainment break-up of the jet core. These droplet sizes are similar to those observed for high gas velocities in the FLECHT SEASET tests [9], and slightly smaller than those observed by Merrington and Richardson [20] at similar relative velocities, for atomization of free water jets flowing in stagnant air or moving air streams.

In an attempt to observe dispersed core droplet sizes beyond the point of wall wetting and the inception of rough wavy annular film flow, a limited number of trials were run using the shortened B2 test section. Near the point of core break-up, large slugs and ligaments from the distorted jet core, created when roll waves expanded to the Pyrex wall, were observed. These larger dispersed liquid masses continued to break-up beyond the jet break-up point, so that at nozzle/test section exit distances roughly twice as long as the jet core break-up length, only dispersed droplets appeared. Most of these droplets had diameters in the range of 0.25-0.55 mm, the same size as the

droplets observed for roll wave crest entrainment. Larger droplets, with diameters of 1-3 mm were also observed, however. These larger droplets are of similar size to those observed for low gas velocities in the FLECHT SEASET tests [9]. Results from this limited number of trials using the shortened test section are not conclusive, since only a small amount of data was obtained. In addition, the effectiveness of the liquid annular film diverter was not established, so that some of the observed droplets may have been formed at the diverter itself. And, finally, the effect of wall wetting makes any observations made beyond the point of jet break-up suspect, when applying them to actual inverted annular flow, where such wetting does not occur.

4. CONCLUSIONS

For this adiabatic simulation of inverted annular flow, the following conclusions can be made:

1. This experimental study was unique in that extensive hydrodynamic information about adiabatic, coaxial jet stability, including liquid core break-up length, break-up mechanisms, core surface characteristics, and dispersed droplet size data was obtained. This data should help in the understanding of film boiling inverted annular flow hydrodynamics. In addition, this data may help in the understanding of the drag-induced break-up of free liquid jets, since jet velocity and relative velocity at the gas/liquid interface were separate variables in this experiment.

2. From preliminary analysis of the data, many similarities can be seen between the phenomenon of coaxial jet disintegration and various aspects of free jet stability, annular and stratified flow, and inverted annular flow film boiling which have been previously investigated [9,13-20]. Results of these previous studies should prove useful in correlating this experimental data.

3. It must be noted that this adiabatic simulation of inverted annular flow, while producing a great deal of useful information, does have certain limitations. First, physical constraints of test section construction limited this study to void fractions no lower than 0.28. Other test section construction and operating constraints limited this study to turbulent liquid core flows, with velocities no lower than 0.7 m/s. Laminar core flow, or low liquid velocities such as those which occur during LWR core reflood, may result in slightly different hydrodynamic behavior. As a third limitation, events beyond the jet core break-up point were not, for the most part, observable, due to wall wetting. Finally, the absence of film boiling conditions (no wall wetting, the presence of an inward-directed radial force at the core surface due to vapor generation) may limit the applicability of these experimental results in the anlaysis of actual inverted annular flow. However, such limitations may be slight, as evidenced by the agreement between droplet size data for this adiabatic simulation and for the FLECHT SEASET heated test section experiments.

ACKNOWLEDGMENTS

This work was performed at Argonne National Laboratory, under the auspices of the U.S. Nuclear Regulatory Commission.

We would like to thank Drs. N. Zuber and M. Young of the NRC for their guidance and assistance in this research, and to thank G. Lambert, E. Sowa and A. Tokuhiro of ANL for help in constructing the experimental apparatus.

NOMENCLATURE

D_J	Jet core diameter
D_o	Gas annulus outer diameter
L_B	Jet core break-up length
v_G	Gas velocity
v_J	Liquid jet core velocity
v_{rel}	Relative velocity ($= \|v_G - v_J\|$)

Greek Symbols

α	Void fraction
λ	Wavelength of maximum growth rate
ρ_G	Gas density

REFERENCES

1. Groeneveld, D.C., "Post-dryout Heat Transfer at Reactor Operating Conditions," presented at the National Meeting on Water Reactor Safety, American Nuclear Society, Salt Lake City, Utah, March 26-28, 1973.

2. Chi, J.W.H., "Slug Flow and Film Boiling of Hydrogen," J. Spacecraft, 1967, Vol. 4, p. 1329.

3. Chen, J.C., Sundaram, R.K., and Ozkaynak, F.T., "A Phenomenological Correlation for Post-CHF Heat Transfer," NUREG-0237, 1977.

4. Laverty, W.F., and Rohsenow, W.M., "Film Boiling of Saturated Nitrogen Flowing in a Vertical Tube," J. Heat Transfer, Trans. ASME, 1967, Vol. 89, p. 90.

5. Kalinin, Ye.K., Berlin, I.I., Kostyuk, V.V., Kochalaev, Yu.S., and Yarkho, S.A., "Heat Transfer in Plug Flow Regime of Film Boiling," Heat Transfer, Soviet Research, 1973, Vol. 5, p. 91.

6. Jensen, R.T., "Inception of Liquid Entrainment During Emergency Cooling of Pressurized Water Reactors," Ph.D. Thesis, Utah State University, 1972.

7. Kurilenko, A.A., Dymenko, S.R., and Kochelaev, Yu.S., "Phase Slip and Heat Transfer to the Liquid in Film Boiling of a Cryogenic Liquid in Piston Flow," J. Eng. Phys., 1980, Vol. 39, p. 961.

8. Ottosen, P., "An Experimental and Theoretical Investigation of Inverse Annular Film Flow and Dispersed Droplet Flow, Important Under LOCA Conditions," Riso National Laboratory, Denmark, Report No. R-424, 1980.

9. Lee, N., Wong, S., Yeh, H.C., and Hochreiter, L.E., "PWR FLECHT SEASET Unblocked Bundle, Forced and Gravity Reflood Task Data Evaluation and Analysis Report, NRC/EPRI/Westinghouse Report No. 10," NUREG/CR-2256, EPRI NP-2013, WCAP-9891, 1981.

10. Iciek, J., "The Hydrodynamics of a Free, Liquid Jet and Their Influence on Direct Contact Heat Transfer - I," Int. J. Multiphase Flow, 1982, Vol. 8, p. 239.

11. Chen, T.-F., and Davis, J.R., "Disintegration of a Turbulent Water Jet," Proc. ASCE, Hyd. Div., 1964, Vol. 90, p. 175.

12. De Jarlais, G., "An Experimental Study of Inverted Annular Flow Hydrodynamics Utilizing an Adiabatic Simulation," M.S. Thesis, Marquette University, Milwaukee, WI, 1983.

13. Miesse, C.C., "Correlation of Experimental Data on the Disintegration of Liquid Jets," Ind. Eng. Chem., 1955, Vol. 47, p. 1690.

14. Grant, R.P., and Middleman, S., "Newtonian Jet Stability," AIChE J., 1966, Vol. 12, p. 669.

15. Lienhard, J.H., and Day, J.B., "The Breakup of Superheated Liquid Jets," J. Basic Eng. Trans. ASME, 1970, Vol. 92, p. 515.

16. Ohnesorge, W., "Die Bildung von Tropfen an Dusen und die Anflosung flussiger Strahlen," Z. Angew Math. Mech., 1936, Vol. 16, p. 355.

17. Ishii, M., and Grolmes, M.A., "Inception Criteria for Droplet Entrainment in Two-Phase Cocurrent Film Flow," AIChE J., 1975, Vol. 21, p. 308.

18. Mishima, K., and Ishii, M., "Theoretical Prediction of Slug Formation in a Horizontal Duct based on Nonlinear Wave Analysis," ANL/RAS/LWR 79-6, 1979.

19. Lord Rayleigh, "On the Instability of Jets," Proc. Lond. Math. Soc., 1878, Vol. 10, p. 4.

20. Merrington, A.C. and Richardson, E.G., "The Break-up of Liquid Jets," Proc. Phys. Soc., 1947, Vol. 59, p. 1.

DISCLAIMER